2116–2129 *Nucleic Acids Research, 2011, Vol. 39, No. 6* *Published online 9 November 2010*
doi:10.1093/nar/gkq923

Characterization of the relationship between integrase, excisionase and antirepressor activities associated with a superinfecting Shiga toxin encoding bacteriophage

P. C. M. Fogg[1], D. J. Rigden[2], J. R. Saunders[1], A. J. McCarthy[1] and H. E. Allison[1,*]

[1]Microbiology Research Group, School of Biological Sciences, University of Liverpool and [2]Structural Biology Group, School of Biological Sciences, University of Liverpool, BioSciences Building, Crown Street, Liverpool L69 7ZB, UK

Received August 24, 2010; Revised September 23, 2010; Accepted September 24, 2010

ABSTRACT

Shigatoxigenic *Escherichia coli* emerged as new food borne pathogens in the early 1980s, primarily driven by the dispersal of Shiga toxin-encoding lambdoid bacteriophages. At least some of these Stx phages display superinfection phenotypes, which differ significantly from lambda phage itself, driving through *in situ* recombination further phage evolution, increasing host range and potentially increasing the host's pathogenic profile. Here, increasing levels of Stx phage $\Phi24_B$ integrase expression in multiple lysogen cultures are demonstrated along with apparently negligible repression of integrase expression by the cognate CI repressor. The $\Phi24_B$ *int* transcription start site and promoter region were identified and found to differ from *in silico* predictions. The unidirectional activity of this integrase was determined in an *in situ,* inducible tri-partite reaction. This indicated that $\Phi24_B$ must encode a novel directionality factor that is controlling excision events during prophage induction. This excisionase was subsequently identified and characterized through complementation experiments. In addition, the previous proposal that a putative antirepressor was responsible for the lack of immunity to superinfection through inactivation of CI has been revisited and a new hypothesis involving the role of this protein in promoting efficient induction of the $\Phi24_B$ prophage is proposed.

INTRODUCTION

Shigatoxigenic *Escherichia coli* (STEC) emerged in the early 1980s as the causal agents of a variety of clinical symptoms and sequelae ranging from mild diarrhea through to life threatening conditions such as hemolytic uremic syndrome (HUS) and thrombotic thrombocytopenic purpura (TTP) (1). The most prevalent STEC strains in the UK, North America and Japan belong to the infamous O157:H7 serogroup (2–4), though several other serogroups dominate mainland Europe and South America (5,6). The most notable non-O157 serogroups known to be strongly associated with human outbreaks are O26 (7), O111 (8) and O145 (9). STEC are characterized by carriage of numerous pathogenicity determinants, but it is the presence of Stx-phages, encoding the eponymous Shiga toxins (Stx) (10,11), which is without doubt the primary factor responsible for the most serious disease manifestations. Significantly, these Stx-phages also have the ability to convert non-pathogenic, commensal bacteria into toxin producers, thus augmenting disease progression (10,12,13).

Stx-phages are classified as lambdoid and, as such, are characteristically temperate and encode an immunity system analogous to bacteriophage lambda (14,15). Immediately after bacteriophage entry into a host cell, Stx-phage can follow either a lytic or lysogenic replication strategy, with the latter resulting in site-directed integration of the phage genome into the bacterial chromosome to generate a prophage, which later can be induced to enter the lytic replication route if exposed to an appropriate induction signal (16). Establishment of lysogeny requires bacteriophage expression of integrase (Int). Usually, the integrases encoded by lambdoid phages are

*To whom correspondence should be addressed. Tel: +44 151 795 4571; Fax: +44 151 795 4410; Email: hallison@liv.ac.uk
Present address:
P.C.M. Fogg, Department of Microbiology and Immunology, University of British Columbia, Vancouver, British Columbia, Canada.

tyrosine recombinases, which, during phage integration, form an Int/DNA intasome complex to catalyze unidirectional creation and resolution of a four way Holliday junction, ultimately yielding an integrated prophage (17). Integrase is the only phage-encoded protein required to facilitate this reaction. Once integrated, the lambdoid prophage produces a repressor (CI), which self-regulates its own promoter and inhibits all other phage gene expression in the lysogen plus any additional incoming homoimmune phage, thus maintaining stable lysogeny and precluding superinfection (15). However, contrary to expectations, various different Stx-phages have been described that are able to circumvent superinfection immunity at high frequency (18,19). The Stx-phage, $\Phi24_B$, can integrate into a single host at least three times, consecutively, with increasing efficiency during each successive infection (20). Multiple infections of this nature may lead to amplified toxin production resulting from a greater *stx* gene copy number and increased opportunity for intracellular recombination with consequent evolutionary implications (21,22). $\Phi24_B$ also encodes a putative antirepressor gene, *ant*, which shares 82% C-terminal identity to the archetypal antirepressor of the *Salmonella* bacteriophage P22 (20). Under normal conditions, the P22 antirepressor is not expressed and superinfection events are blocked, but under conditions that enable its expression, the P22 antirepressor binds and inactivates the P22 repressor protein, CII (23–25). Furthermore, the P22 Ant is also effective against the homologous λ repressor CI (24). This Ant-mediated repressor inactivation is a potential mechanism to explain the lack of superinfection immunity in $\Phi24_B$ (20).

Under certain conditions, such as DNA damage, an integrated phage may be induced to excise itself from the host genome and enter the lytic replication cycle. Activated RecA (part of the host SOS response) induces autocleavage of the repressor (26), allowing infective phage particles to be produced. Similarly to integration, bacteriophage excision is also catalyzed by integrase, though a phage-encoded excisionase is required additionally to control directionality of the reaction (Xis or recombination directionality factor, RDF) (27,28). RDFs may control the fate of the integrase-catalyzed reaction by directly interacting with the intasome, facilitating an allosteric change which favors excision (29), or alternatively, they may act as transcriptional activators, inducing expression of their cognate integrases thereby promoting phage excision (28). In most cases, an RDF/Xis factor is necessary to enable excision of an integrated stretch of DNA. There is a single case, described in association with a pathogenicity island, where an integrase is able to catalyze integration and excision reactions, independent of a specific excisionase (30,31), but this has never been described for an infective phage.

Preliminary qualitative RT–PCR data revealed that Stx-phage $\Phi24_B$ weakly expresses a putative antirepressor in uninduced lysogen cells (20). Moreover, these cells also unexpectedly express *int* indicating that integrase production may not be fully repressed in lysogen cells. These two observations support alternative hypotheses to explain establishment of multiple lysogeny by Stx-phages, antirepressor or integrase mediated, respectively. Here, we demonstrate increasing levels of $\Phi24_B$ integrase expression in multiple lysogen cultures and apparently negligible repression of *int* expression by CI. The $\Phi24_B$ *int* transcription start site and promoter region were determined and found to differ from *in silico* predictions (20). We also confirm activity of this integrase in the integration reaction but rule out the possibility that it can catalyze excision in the absence of a phage directionality factor, despite the absence of an obvious associated excisionase in the $\Phi24_B$ genome. Subsequently, we located a novel excisionase gene, identified through genetic complementation assays when co-expressed with $\Phi24_B$ *int*. In addition, the previous proposal of a putative antirepressor affect on superinfection immunity is revisited and a new hypothesis put forward.

MATERIALS AND METHODS

Bacterial strains, bacteriophages and media

The bacterial strains, bacteriophages and plasmids used in this study are listed in Table 1. *Escherichia coli* K-12 strain MC1061 was the host of choice for bacteriophage infection and lysogen production. JM109-λ pir was the propagation strain for the suicide plasmid pKNG101, while Invitrogen One Shot TOP10 cells were used for all cloning and recombination assays, except where the plasmid p$\Phi24_B$-IX was used, which required the use of *E. coli* strain BL21(AI) to control the expression of excisionase under its inducible T7 promoter. Bacteria were routinely cultured in phage buffer [2.5% (w/v) Luria–Bertani (LB) broth (Merck) with 0.01 M $CaCl_2$] or on LB agar plates [2.5% LB broth plus 1.5% (w/v) agar (Merck)]. Where appropriate, the following antibiotics were added ($\mu g\,ml^{-1}$): rifampicin (3500), ampicillin (100), kanamycin (50), chloramphenicol (50) and spectinomycin (100).

Antirepressor knockout

The 'putative' $\Phi24_B$ antirepressor was amplified using Ant F/R primers (Supplementary Table S1). The resulting PCR product and the suicide vector pKNG101 were cut with BamHI restriction endonucleases, agarose gel purified and recovered with the QIAquick gel extraction kit. The two purified DNA fragments were ligated together to produce pKNG-*ant* (Table 1). Selected transformants were used as a template for inverse PCR using Ant Inv F/R primers (Supplementary Table S1), while the *aadA* spectinomycin resistance cassette was also amplified with *aadA* F/R AccI (Supplementary Table S1). Both PCR products were purified and cut with the restriction endonuclease AccI and ligated together to produce pKNG-*antΔ* (Table 1). pKNG-*antΔ* was transformed into electrocompetent MC1061 lysogen cells carrying either of the prophages $\Phi24_B$::Kan and $\Phi24_B$::Cat (Table 1). All Sm^R resistant transformant colonies contained pKNG-*antΔ* integrated into $\Phi24_B$ *ant*, as confirmed by the absence of a PCR amplification product with Ant F/R primers and sensitivity to sucrose when subcultured on LB Agar plates in which NaCl was

Table 1. Bacteria/phage strains and plasmids used in this study

Strain/Plasmid	Description	References
MC1061	*E. coli* K-12 derivative	(83)
DM1187	*E. coli* K-12 derivative, *recA441*	(84)
JM109 λ pir	*E. coli* K-12 derivative, λ pir	(85)
$\Phi24_B$::Kan	Stx-phage, $stxA_2$*Δaph3*	(18)
$\Phi24_B$::Cat	Stx-phage, $stxA_2$*Δcat*	
$\Phi24_B$::Spec	Stx-phage, $stxA_2$*ΔaadA*	(20)
$\Phi24_B$::Kan *antΔ*	Stx-phage, $stxA_2$Δaph3, antΔaadA	This study
OneShot TOP10	Competent cells, *recA*-	Invitrogen
BL21(AI)	araB::T7RNAP-tetA, recA-	
pBAD/*Myc*-His C	araBAD, C-*myc*/His6 epitope, pBR322 ori, Am^R	
pKNG101	R6K Ori, *sacB*, Sm^R	(86)
pACYC-Duet	P15A ori, Cm^R	Novagen, EMD
pCDF-Duet	CDF ori, Sp/Sm^R	
p$\Phi24_B$-*cI*	pBAD carrying $\Phi24_B$ *cI*	This study
p$\Phi24_B$-*int*	pBAD carrying $\Phi24_B$ *int*	
p$\Phi24_B$-*attB*	pACYC-Duet carrying $\Phi24_B$ *attB*	
p$\Phi24_B$-*attP*	pCDF-Duet carrying $\Phi24_B$ *attP*	
p$\Phi24_B$-*attBP*	p$\Phi24_B$-*attP* integrated into p$\Phi24_B$-*attB*	
p$\Phi24_B$-X	pACYC carrying $\Phi24_B$ *xis*	
p$\Phi24_B$-IX	p$\Phi24_B$-*int* carrying $\Phi24_B$ *xis*	
p$\Phi24_B$-*ant*	pBAD carrying $\Phi24_B$ *ant*	
pKNG-*ant*	pKNG101 carrying $\Phi24_B$ *ant*	
pKNG-*antΔ*	pKNG101 carrying $\Phi24_B$ *antΔaadA*	
pStxACYC	pACYC-Duet carrying $\Phi24_B$ *pR′-luxABCDE* fusion	

ant: putative antirepressor; *int*: integrase; cI: phage repressor; *attB*: phage insertion site within the MC1061 chromosome utilized by $\Phi24_B$; *attP*: $\Phi24_B$ phage attachment site; *xis*: excisionase; $stxA_2$: Shiga toxin A sub-unit for Stx2; *aph3*: kanamycin resistance gene (Kan^R); *aadA*: spectinomycin resistance gene (Sp^R/Sm^R); *cat*: chloramphenicol acetyl transferase gene (Cm^R); *luxABCDE: Photorhabdus luminescens* bioluminescence operon; *recA*$^-$: mutation in DNA repair recombinase gene; *recA441*: mutation in *recA* leading to constitutive activation; λ pir: chromosomal copy of the bacteriophage lambda replication initiation protein; R6K ori: λ pir dependent plasmid origin of replication; *tetA*: tetracycline resistance; *ara*B/araBAD: arabinose inducible promoter; T7RNAP: bacteriophage T7 RNA polymerase; His6: C-terminal hexa-histidine tag; C-*myc*: C-terminal *myc* human oncogene peptide epitope; *sacB*: levansucrase, a conditional lethal gene; *ori*: origin of replication; *pR′*: $\Phi24_B$ late gene promoter.).

replaced with 10% (w/v) sucrose. Randomly selected colonies were passaged in LB broth without antibiotic selection, and 100 µl of mid-exponential culture was spread, daily, onto LB Sucrose Agar plates. Any colonies able to grow in the presence of sucrose had lost the integrated pKNG101 plasmid backbone, and the wild-type *ant* was replaced by *antΔaadA*, as confirmed by PCR (data not shown).

Luminescent reporter gene fusion construction

The $\Phi24_B$ *pR′* promoter region was amplified from purified $\Phi24_B$ DNA using pStx F/R oligonucleotides (Supplementary Table S1) and the *luxABCDE* operon was amplified from pSB2030 (32) using Lux F/R primers (Supplementary Table S1). Both the promoter and *lux* operon were cut with the relevant restriction enzymes (PstI, SpeI and XhoI), while the medium copy number plasmid pACYC-Duet (Table 1) was cut with PstI and XhoI. Each of the above was agarose gel purified and recovered using the QIAquick gel extraction kit (Qiagen, Ltd). A single plasmid, pStxACYC, was constructed following ligation of the three products, (Table 1). pStxACYC was then transformed into competent MC1061/$\Phi24_B$::Kan or MC1061/$\Phi24_B$::Kan *antΔ* lysogen cells (Table 1); transformants were selected for on agar plates containing chloramphenicol (50 µg ml^{-1}) and spectinomycin (100 µg ml^{-1}). Complementation of *ant* was performed by amplifying the $\Phi24_B$ *ant* gene from purified bacteriophage $\Phi24_B$ DNA using Ant F/R oligonucleotides (Supplementary Table S1). This product was agarose gel purified and cut with the restriction endonucleases NcoI and SalI, whilst the plasmid pBAD/*Myc*-His was cut with the same enzymes (Table 1). Both products were ligated together to create the antirepressor expression construct, p$\Phi24_B$-*ant* (Table 1). p$\Phi24_B$-*ant* was then transformed into competent $\Phi24_B$::Kan *antΔ* lysogen cells harboring pStxACYC.

Lux reporter gene assay

Fresh overnight cultures were used to inoculate 50 ml of LB broth; each culture was prepared in duplicate—one culture serving as a negative control and the other subjected to norfloxacin-based bacteriophage induction (33). Cultures were grown for ~3 h to mid-exponential growth phase ($OD_{600} = 0.5$), at which point the antibiotic norfloxacin was added to the induced cultures at a working concentration of 1 µg ml^{-1}. Triplicate 200 µl samples were taken immediately for luminescence and optical density measurements, in opaque and transparent 96-well plates, respectively, and analyzed in a VICTOR3 plate reader (PerkinElmer). This sampling regime was repeated at intervals of 30 min. Specific luminescence was calculated as luminescence per optical density unit.

Quantitative PCR

Single, double and triple lysogen cultures were harvested at an OD_{600} of 0.5. Total RNA was extracted using an RNeasy mini kit (Qiagen Ltd), according to the manufacturer's specifications. Genomic DNA contamination was removed with Ambion RNase-free DNase (Applied Biosystems) and RNA was quantified with a NanoDrop ND-1000 spectrophotometer (Thermo Fisher Scientific Inc.). RNA (0.5 µg) for each reaction was transcribed into cDNA using RNaseH reverse transcriptase (Bioline Ltd) in a total of 20 µl. cDNA (1 µl) was then used as template for each qPCR reaction in Sensimix qPCR reaction mixture (Quantace Ltd). All experiments were designed to comply with the standard Sensimix cycling conditions with an annealing temperature of 60°C and an amplicon size of ~100 bp. qPCR reactions were carried out using a Miniopticon thermal cycler (BioRad Labs Inc.). Integrase was amplified using *int* qPCR F/R, and the copy number was determined on a standard curve (copy number range = $5 \times 10^3 - 5 \times 10^8$), providing absolute quantification of the amplified products.

CI overexpression

$\Phi24_B$ *cI* was amplified from bacteriophage $\Phi24_B$ DNA purified according to the method of Rooks *et al.* (34) using CI F/R oligonucleotides (Supplementary Table S1), agarose gel purified and cut with NcoI and SalI restriction endonucleases; the plasmid pBAD/*Myc*-His was also cut with NcoI and SalI (Table 1). These products were ligated together to create p$\Phi24_B$-*cI* (Table 1). p$\Phi24_B$-*cI* was then transformed into competent *E. coli* lysogen cells [strain MC1061 carrying the $\Phi24_B$::Kan prophage (MC1061/$\Phi24_B$::Kan)], and transformants were selected for by resistance to the antibiotics kanamycin (50 μg ml^{-1}) and ampicillin (100 μg ml^{-1}). A MC1061/$\Phi24_B$::Kan culture carrying p$\Phi24_B$-*cI* was incubated at 37°C until it reached an OD_{600} of 0.5, and *cI* expression was induced through addition of arabinose to working concentrations of 0.2% (w/v), 0.002% (w/v) or 0% (negative control), before further incubation at 37°C for 2 h. Samples were taken post-induction and processed for qPCR, as above, and for SDS–PAGE analysis. Transcripts of the *cI*, *Q* and *int* genes were amplified with *cI* qPCR F/R, *Q* qPCR F/R and *int* qPCR F/R, respectively (Supplementary Table S1); an endogenous reference, 16S rRNA processing gene *rimM*, was amplified with *16S* qPCR F/R (Supplementary Table S1). Expression from test strains was quantified by the $2^{-\Delta\Delta C_T}$ relative abundance method (35).

Rapid amplification of 5′-complementary DNA ends (5′-RACE)

The lysogen MC1061/$\Phi24_B$::Kan was cultured at 37°C to an OD_{600} of 0.5. Total RNA was extracted using an RNeasy mini kit, and immediately processed with a 2nd generation 5′/3′-RACE kit (Roche Applied Science) according to manufacturer's instructions for 5′-amplification. DNA purification steps were carried out using the manufacturer's recommended High Pure PCR Product Purification Kit (Roche Applied Science), and the custom oligonucleotide primers Int RACE Sp3, Sp2 and Sp1 (Supplementary Table S1) were used in conjunction with primers included in the 5′/3′-RACE kit for amplification of the 5′-integrase region. The resultant PCR amplification products were cloned into a ZeroBlunt vector (Invitrogen) and sequenced using standard M13 F/R primers (GATC-Biotech). The transcription start site was mapped onto the $\Phi24_B$ genome, and the promoter region and binding sites predicted *in silico*.

Integration/excision vector construction

The $\Phi24_B$ *int* and *attP* sites along with its primary bacterial *attB* site were amplified with Integrase F/R, attP F/R and attB F/R, respectively (20). The integrase gene and the two attachment sites were each cloned, separately, into ZeroBlunt cloning vector (Invitrogen), according to manufacturer's guidelines. The cloned fragments were subsequently excised using NcoI and KpnI, or BamHI and XhoI endonucleases for the integrase gene or both the attachment sites, respectively. Three plasmids with compatible origins of replication were also cut, pBAD/*Myc*-His C (NcoI and KpnI), pACYC-Duet and pCDF-Duet (BamHI and XhoI) (Table 1). After deactivation of the enzymes, the integrase gene was ligated into pBAD/*Myc*-His C to form p$\Phi24_B$-*int* (Table 1), *attB* was ligated into pACYC-Duet to form p$\Phi24_B$-*attB* (Table 1) and *attP* was ligated into pCDF-Duet to form p$\Phi24_B$-*attP* (Table 1).

Table 2. Integration/excision plasmid permutations

Assay	p$\Phi24_B$-*attB*	p$\Phi24_B$-*attP*	p$\Phi24_B$-*attLR*	p$\Phi24_B$-*int*	p$\Phi24_B$-IX	$\Phi24_B$
1	+	+	−	−	−	−
2	+	+	−	+	−	−
3	−	−	+	−	−	−
4	−	−	+	+	−	−
5	−	−	+	−	+	−
6	+	+	−	−	−	+
7	−	−	+	−	−	+

A summary of the various combinations of plasmids used for recombination assays to assess the function $\Phi24_B$ integrase and excisionase. All of the assays summarised above were carried out in *recA*$^-$ *E. coli* hosts. Plasmid components (**p$\Phi24_B$-*attB*, p$\Phi24_B$-*attP*, p$\Phi24_B$-*attLR*, p$\Phi24_B$-*int* and p$\Phi24_B$-IX**) are described in Table 1, whilst the final column refers to presence/absence of a **$\Phi24_B$** prophage. For all of the assays, cells carrying the plasmids detailed were grown to mid-logarithmic growth phase (OD_{600}:0.5) with the appropriate antibiotic selection. Plasmids from **1**, **3** and **6** were immediately purified with a Plasmid Miniprep kit (Qiagen Ltd). Cultures **2** and **4** were induced with arabinose, whilst **5** was induced with arabinose [0, 0.2 and 0.02 (w/v)] and IPTG (1 mM), each for 2 h, before plasmids were purified. Culture **7** was induced to produce native excisionase by addition of 1 μg ml^{-1} norfloxacin for 2 h, prior to plasmid purification.

Integration/excision assay

Various combinations of plasmid constructs in appropriate strains were produced as summarized in Table 2. Integration of pΦ24B-*attP* into pΦ24B-*attB* to create pΦ24B-*attLR* (Table 1) under different conditions was monitored qualitatively by plasmid purification using a Plasmid Miniprep kit (Qiagen) and visualization on a 0.7% (w/v) agarose gel and quantitatively by qPCR using linearized (digestion with either BglI or PciI) plasmids as templates with integration specific primers that spanned the crossover site [Integ qPCR F/R (Supplementary Table S1)] as well as primers specific to the plasmid backbone [Duet qPCR F/R (Supplementary Table S1)]. Integration and excision events were then compared by the relative abundance of the integrated amplification product (Integ qPCR F/R derived product) compared to the total plasmid copy number present (Duet qPCR F/R derived product). qPCR was carried out using a 7500 Fast qPCR system (Applied Biosystems) and Sensimix qPCR reagents (Quantace Ltd, see Quantitative PCR).

Excisionase cloning and expression

The putative excisionase was initially identified by a systematic *in silico* screening process, based solely on size and location of possible ORFs. All potential ORFs of 150–600 bp, within 5 kb of $\Phi24_B$ *int* and beginning with any of the *E. coli* alternate start codons [ATG, GTG, TTG, ATT and CTG (36)], were analyzed. The candidate Xis

was amplified from $\Phi24_B$ DNA using Xis F/R oligonucleotides (Supplementary Table S1), purified and cut with the restriction endonucleases NcoI and BamHI. pACYC-Duet (Table 1) was also cut with the same enzymes, NcoI and BamHI. The two compatible DNA fragments were ligated together to produce p$\Phi24_B$-X (Table 1). p$\Phi24_B$-X was then used as a template for PCR amplification with T7 F/Xis R. The resulting PCR product, containing the T7 promoter from pACYC-Duet plus the putative $\Phi24_B$ *xis*, was cut with HindIII endonuclease and ligated into HindIII cut p$\Phi24_B$-*int* (Table 1) to create p$\Phi24_B$-IX (Table 1). p$\Phi24_B$-IX was transformed into BL21(AI) cells (Table 1) and transformants selected for by resistance to ampicillin (100 μg ml^{-1}). Excisionase activity was monitored by agarose gel electrophoresis and qPCR (see Integration/excision assay).

Bioinformatics

Database searching was done with BLAST and PSI-BLAST (37) in the nr database (38). Domain searches were made in the databases CDD (38) and InterPro (39). More sensitive domain searching was done with HHpred (40,41). In accord with the extreme sequence divergence exhibited by the Xis sequences, a structure-based alignment approach was employed. A structure alignment of members of Pfam (42) families Phage_AlpA [PF05930; TorI with PDB (43) code 1zh4 (44)], Excisionase like [PF07825; lambda phage Xis, 2ief (27)] and PF09035 [Tn916-Xis; 1y6u (45)] was made with MUSTANG and STACCATO (46) and used, as the basis to unite three alignments using the program Jalview (47). Each of the three alignments, made with MUSCLE (48), contained Xis sequences bearing similarity to the respective Pfam families. Other Xis sequences, belonging to different Pfam families but recognizably distantly related to AlpA, were added to the aggregate alignment with the benefit of alignments deriving from the sensitive profile–profile matching program HHpred (40,41). The resulting alignment was subject to phylogenetic analysis with MEGA 4 as follows (49). The bootstrap consensus tree inferred from 1000 replicates was taken to represent the evolutionary history of the taxa analyzed (50). The evolutionary distances were computed using the Poisson correction method (51) and the units are the number of amino acid substitutions per site. The ME tree was searched using the Close-Neighbor-Interchange (CNI) algorithm (52) at a search level of 1. The Neighbor-Joining algorithm (53) was used to generate the initial tree. All positions containing alignment gaps and missing data were eliminated only in pair-wise sequence comparisons.

Ten models of $\Phi24_B$ Xis were produced with MODELLER (54) using the structure of TorI [PDB code 1zh4 (44)] as a template. The DOPE statistical potential (55) and stereochemical analysis (56) were used to select a model for further analysis. Electrostatic characteristics of the model were explored with APBS (57) and putative protein–protein interfaces sought with HotPatch (58). DNA-binding ability was tested with DB-MOM (59) and PRO-DNA (60). Further protein structure superpositions were done with SSM (61) and displayed in PyMOL (62), which was also used to produce structure figures.

RESULTS

Characterization of the activity of ant

Previous studies have shown that the frequency of multiple lysogen formation, through sequential superinfection, exceeds the rate of single lysogen formation by infection of a naïve host (19,20). This suggests that the incumbent prophage in some way aids the integration of the superinfecting bacteriophage, thus increasing integration efficiency. The presence (Figure 1A) and expression of a putative antirepressor gene (*ant*) present in $\Phi24_B$ was postulated to be responsible for the phenomenon of multiple lysogeny through a mechanism of derepression (20). However, superinfection experiments using $\Phi24_B$ *antΔ* strains demonstrated that the lack of Ant failed to have any effect, positive or negative, on superinfection compared with wild-type $\Phi24_B$ (data not shown). Instead, further investigation has produced evidence of a likely role in assisting relief of CI repression during induction into the lytic cycle, consistent with independent observations reported for a similar antirepressor of bacteriophage 2851 (63). A pR′-*luxABCDE* fusion was used as a reporter for bacteriophage late gene expression following norfloxacin induction of lysis (Figure 1B). Three different lysogen cultures were tested: $\Phi24_B$ wild-type, $\Phi24_B$ *antΔ* and $\Phi24_B$ *antΔ* complemented with pBAD-*ant*. Luminescence was measured over 4 h proceeding norfloxacin addition. The lag phase before substantial increases in pR′ expression were detectable was ~120 min for each of the strains, and the difference between both the two test strains and the wild-type reference varied markedly from this time point onwards (Figure 1C). The *antΔ* strain peaked at luminescence intensity up to 55.6% of the wild-type luminescence at 120 min, but decreased to 27.2–31.0% for the remainder of the experiment (Figure 1C). In comparison, the complemented strain was able to restore 82.1% of wild-type luminescence levels at 120 min before decreasing to 64.3–65.3% and eventually returning to 79.5% after 240 min (Figure 1C).

Uninduced integrase expression

Clearly, some factor outside the production of an antirepressor is involved in driving increased frequencies of lysogen formation upon superinfection. A potential mechanism to explain this observation would be expression of integrase from the resident integrated phage, which would more typically be strongly repressed by the lambdoid immunity system present in Stx-phages. Integrase transcript abundances were determined for single, double and triple lysogens of the Stx-phage by qPCR, in the absence of any stimulus for the lytic cycle. Expression of $\Phi24_B$ integrase increased 2.6-fold in the double lysogen and 7.5-fold in the triple lysogen, each compared to expression levels in the single lysogen (Figure 2A). This observation suggests that integrase expression is not fully controlled by the global phage

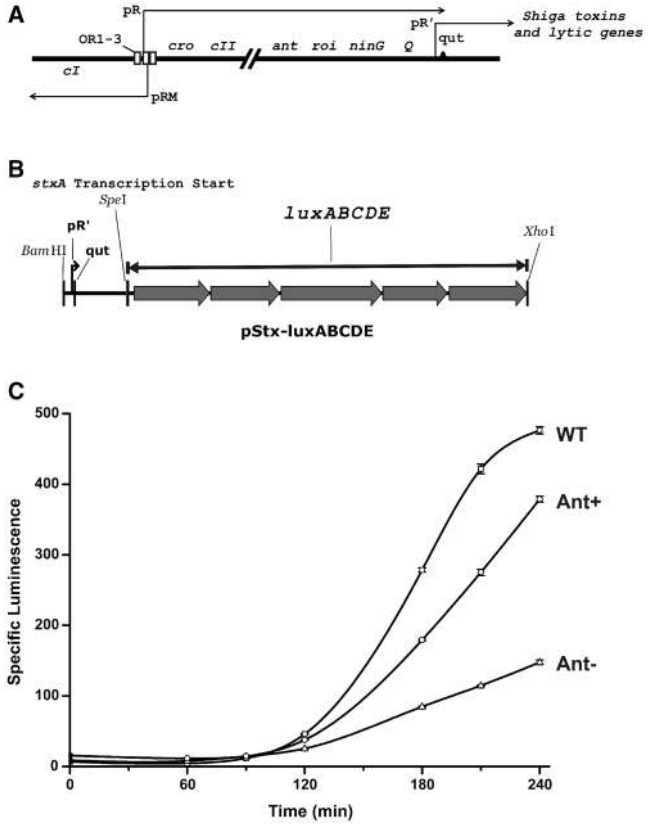

Figure 1. Antirepressor Location and Function. (**A**) Transcription is indicated by arrows above or below the line with pR, pR′ and pRM promoters labeled adjacent to their transcription start sites. Gene names, indicated in italics, are transcribed leftward when below the line or rightward when above. The right operator region including the 3 CI binding sites (OR1-3) is annotated. The qut transcription termination site is represented by a raised triangle immediately after pR′. The putative antirepressor gene is located before this *qut* site and thus should be expressed shortly after induction to the lytic cycle, where it plays a role in accelerating phage derepression. Relief of CI mediated repression results in high level expression from pR′ leading irreversibly to lysis and release of Stx. (**B**) Map of the pR′ reporter gene fusion, including the *stxA* transcription start site. The pR′ promoter location and the *qut* transcription termination site are indicated. (**C**) Lux specific luminescence driven from the pR′ promoter during induction of phage lysis by addition of norfloxacin antibiotic. T_0 is measured from the addition of inducing agent and there is a 90-120 min lag phase before expression increases appreciably. The three lines correspond to the antirepressor knock-out mutant (Δ, Ant−), the complemented strain (○, Ant+) and the wild-type control (□, WT). Error bars represent combined standard error for luminescence/optical density quotient ($n = 3$).

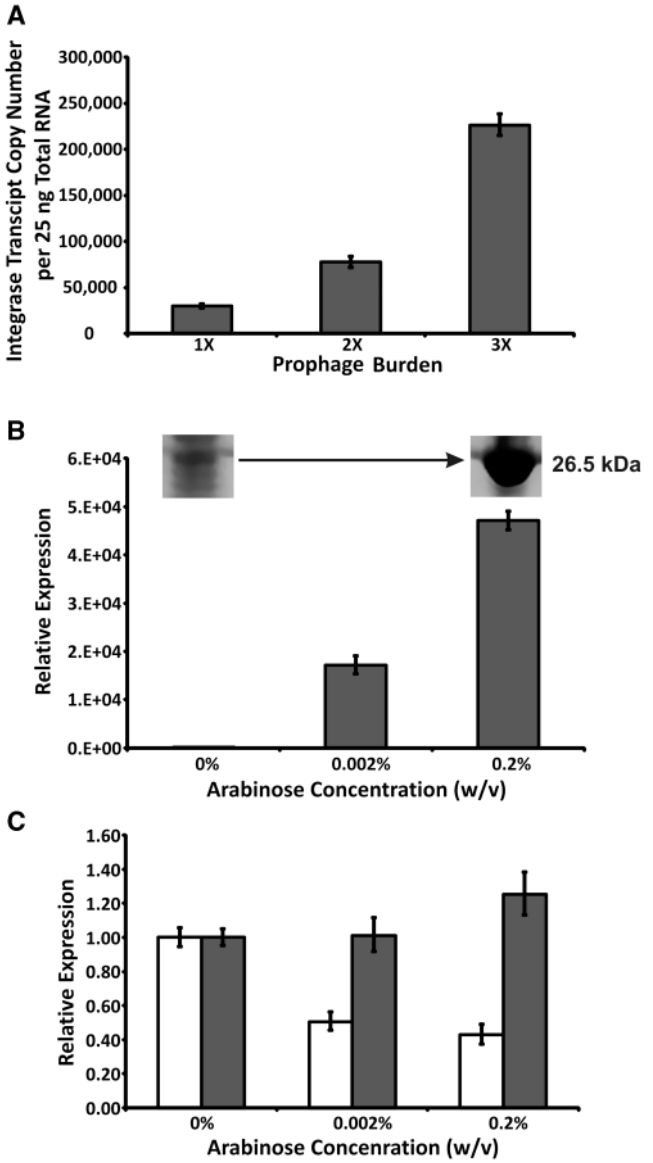

Figure 2. (**A**) $\Phi24_B$ integrase expression. Absolute qPCR quantification of integrase mRNA copy numbers in uninduced, mid-exponential growth phase single (1X), double (2X) and triple (3X) lysogen cultures. (**B**) $\Phi24_B$ CI overexpression. Relative qPCR quantification of $\Phi24_B$ *cI* repressor transcripts overexpressed from an *araBAD* promoter in the presence of increasing concentrations of arabinose from 0% to 0.2% (w/v), including an overlaid 12% SDS-PAGE gel confirmation of protein level overexpression. (**C**) Relative qPCR quantification of *Q* and *int*. Determination of the relative levels of expression of the $\Phi24_B$ lytic regulator *Q* (open bars) and *int* (closed bars) genes in the presence of arabinose-induced *CI* repressor.

repressor protein, CI. Furthermore, complete genome sequence data for $\Phi24_B$ (Accession number: HM_208303) has revealed that the integrase gene is present in an inverted orientation (Figure 3A) compared to other lambdoid phages such as lambda (NC_001416) and 933W (NC_000924). This inversion implies that its regulation must be different to these well-studied phages like Lambda phage where the *int* gene is subject to repression from CI. To identify whether the regulation of $\Phi24_B$ Int expression is uncoupled from CI repression, CI was overexpressed through arabinose induction (Figure 2B) in a $\Phi24_B$ lysogen background, and the effect on integrase expression monitored by qPCR (Figure 2C). As a control, expression of the *Q* antiterminator gene, the key regulator of the lytic cycle, was also monitored (Figure 2C). As expected, integrase expression was not affected by increased levels of CI, whereas Q expression was significantly ($P < 0.05$) decreased (Figure 2B and C). The $\Phi24_B$ immunity region, whilst identical to bacteriophage 933W (20,64), differs in organization from bacteriophage lambda in that there are only two left operator binding

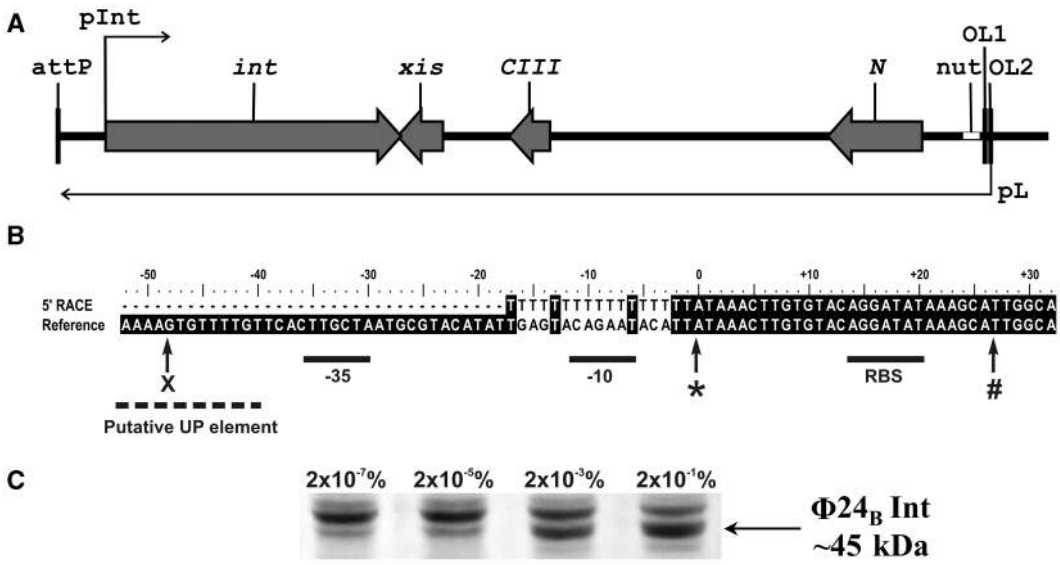

Figure 3. (**A**) Schematic map of the $\Phi24_B$ integrase region. This updated genetic map includes the integrase in an inverted orientation to the bacteriophage lambda model, and thus not under the control of CI through its indirect repression of *int* transcription from pL during lysogeny (as in lambda), and the novel excisionase ORF which would be under the auspices of CI via pL. The proposed pInt promoter is also indicated. (**B**) Schematic of the $\Phi24_B$ integrase transcription start site and predicted promoter as determined by 5′-RACE and *in silico* analysis. The poly-T start to the RACE output (5′-RACE) is an artifact of the amplification process; $\Phi24_B$ genome sequence (HM_208303) was used for the alignment. Putative -10/-35 promoter constituents and the distal portion of a putative UP-element are indicated by labeled solid lines and a dashed line, respectively. Transcription start is also indicated by asterisks along with the new putative translational start site hash and ribosomal binding site (RBS) along with the previous, discredited translational start site (X). (**C**) Expression of $\Phi24_B$ integrase from an *araBAD* inducible promoter with increasing levels of arabinose, shown by 10% SDS–PAGE.

regions rather than three. This does not however compromise repression of transcription from the pL promoter or affect lysogen stability (65,66). Bandshift analysis was carried out to confirm that the $\Phi24_B$ CI protein is able to effectively bind to the left operator region. Indeed, similar to 933W (67), binding occurred as expected (data not shown), and thus a defect in the immunity region is unlikely to be a factor in the phenomenon of multiple lysogeny.

5′-RACE determination of integrase start site

$\Phi24_B$ encodes a novel integrase, as yet uncharacterized, which is extremely promiscuous with regard to integration site selection (20). Furthermore, there was no obvious gene encoding an excisionase-like protein identifiable anywhere on the bacteriophage chromosome (HM_208303), including the areas immediately up- and down stream of the *int* gene. An integrase capable of performing both excision and integration functions has been described in association with an *E. coli* pathogenicity island (31), but never in association with an inducible bacteriophage, lambdoid or otherwise. *In silico* analysis predicted a 1245 bp integrase-encoding ORF in the $\Phi24_B$ genome, and this was cloned into a pBAD expression vector (Invitrogen). However, we failed to successfully express the integrase protein after repeated attempts (data not shown). We therefore set out to establish the transcription and translation start sites, and determine whether these were compatible with the *in silico* predictions. To resolve the transcriptional start site, rapid amplification of the 5′-complementary DNA end (5′-RACE, Roche) was performed. The cDNA end product was sequenced and revealed that transcription actually initiates 46-bp downstream of the expected translational start codon (Figure 3B). From this information, the promoter elements were predicted using the BDGP neural network promoter predictor (68) and a potential UP-transcription activation element was mapped by comparison to published sequences (69,70). UP elements are short stretches of AT-rich sequence present in some promoters, directly upstream of the core region. These elements enhance transcription by interacting with RNA polymerase, though they are not essential for overall promoter function (69–71). The $\Phi24_B$ integrase promoter (*pInt*) contains a match to only the distal section of the UP element consensus sequence (9 out of 11 bases) and the proximal section is absent, however, 'half sites' have previously been shown to be functional (72). Improved promoter and transcriptional start data also assisted in the production of a new *int* ORF prediction using the FrameD online 'Gene Finder' tool (http://bioinfo.genotoul.fr/apps/FrameD/FD) (73). This updated ORF utilizes the rare TTG start codon and experimentally facilitated Int expression from an inducible promoter (Figure 3C) (73).

Integration excision system: integrase inability to catalyze excision

In order to test Int function experimentally, a three-plasmid system was used in which the $\Phi24_B$ *attP* site, bacterial *attB* site and the $\Phi24_B$ integrase were each cloned separately into compatible, low copy number

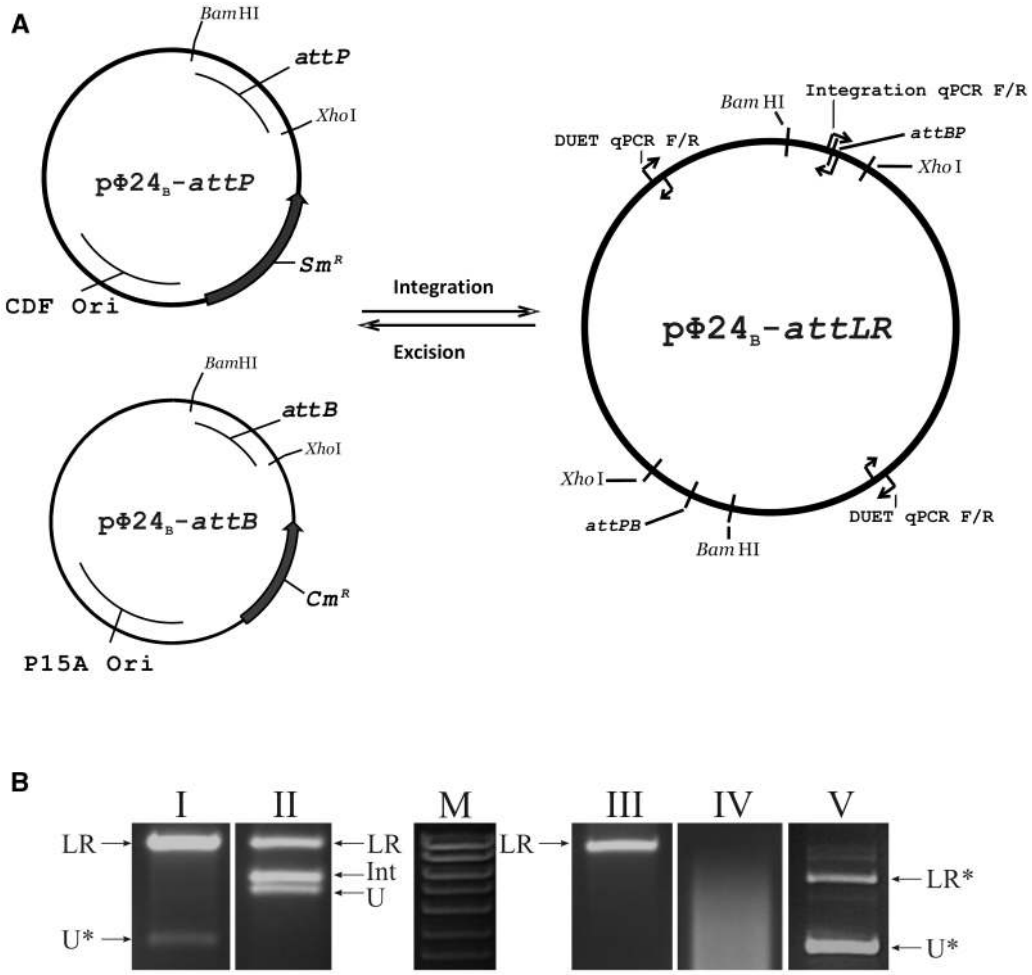

Figure 4. Plasmid integration/excision assay. (**A**) Schematic representation of the component plasmids bearing the $\Phi24_B$ attachment sites (p$\Phi24_B$-*attB* and p$\Phi24_B$-*attP*) and the combined integrant resulting from integrase mediated, site-directed recombination (p$\Phi24_B$-*attLR*). qPCR primer binding sites are highlighted on the integrated p$\Phi24_B$-*attLR* plasmid. (**B**) Agarose gel electrophoresis of purified plasmids harvested following the *in situ* integration or excision assays. The panels correspond to: (**I**) plasmid integration in the presence of a $\Phi24_B$ lysogen (Table 2, assay 6); (**II**) integrase expressed from an inducible promoter (Table 2, assay2); (**M**) Bioline Hyperladder I is included as a size reference; (**III**) excision control without integrase or excisionase (Table 2, assay 5, no arabinose); (**IV** and **V**) integrase plus excisionase (Table 2, assay 5, with arabinose). Arrows indicate the position for the plasmids: (**LR**) integrated p$\Phi24_B$-*attLR* plasmid; (**Int**) p$\Phi24_B$-*int*; and (**U**) the similarly sized plasmids p$\Phi24_B$-*attB* and/or p$\Phi24_B$-*attP*. All plasmids were linearized with BglI endonuclease, except where marked by asterisks in lane **V**, which contains supercoiled plasmid DNA. Complete degradation of excised plasmids after attempted linearization is shown in panel **IV**.

plasmids. Integration and excision events could then be detected by determining the presence of either a large p$\Phi24_B$-*attLR* integrated plasmid or individual, resolved p$\Phi24_B$-*attB*/*attP* containing plasmids (Figure 4A), and these could be quantitated further by qPCR. By this method, we were able to demonstrate integrative function for the expressed integrase protein alone, in the absence of any other accessory phage proteins (Table 2 and Figure 4B). Moreover, efficient integration of the plasmids was also observed when transformed into a single lysogen host in the absence of any stimulus for integrase production (Figure 4B). This latter observation further corroborates the hypothesis set out earlier that integrase is expressed in a lysogen, uncoupled from CI mediated repression, and that this may help to assist in the integration of superinfecting bacteriophage. All attempts to resolve the integrated p$\Phi24_B$-*attLR* plasmid into its two component plasmids with the integrase expression construct present, alone, were futile (Table 2, assay 4; data not shown), whilst resolution of p$\Phi24_B$-*attLR* within in a lysogen was easily detectable when that lysogen was subjected to norfloxacin induction (data not shown), but not detectable, even by qPCR, in an uninduced lysogen (Table 2, assay 7). These experiments indicated that there must be a phage-encoded accessory factor that remained coupled to CI repression and the standard lambdoid regulatory cascade that is essential for $\Phi24_B$ prophage excision.

Identification and bioinformatic analysis of a putative excisionase

The small size of the majority of currently described excisionases (typically more than 100 amino acids) limits

the ability to predict and identify novel excisionase proteins based on homology searches (28). Excisionase genes are usually found in close proximity to their cognate *int* (74,75), therefore, due to the location and orientation of $\Phi24_B$ *int*, it was predicted that the excisionase gene was likely to be situated adjacent to the 3′ of the integrase. In addition, although *E. coli* primarily utilizes ATG as a translation start codon (83% of genes in *E. coli* K-12), several other codons can also be used such as GTG (14%) and TTG (3%) as well as the rare ATT and CTG codons (36). Bearing this information in mind, investigation of all possible short ORFs in the proximity of the integrase gene identified only one candidate ORF, which was predicted to encode an 8 kDa protein. Database searches by BLAST and PSI-BLAST revealed only four close homologs from *E. coli* strains, none of which had been experimentally determined to possess an excisionase function. Similarly, searches of domain databases CDD and InterPro with default parameters failed to place the candidate protein sequence in any known protein family. Nevertheless, analysis with HHpred, a more sensitive sequence comparison method, revealed a clear but distant relationship between the candidate ORF and Pfam family phage_AlpA (PF05930). The *e*-value was 5×10^{-6}, and the alignment between the ORF and the domain consensus produced 40% sequence identity, although the alignment only covered 47 residues of the candidate ORF. This provided a strong indication that the candidate ORF indeed encoded a Xis protein since several characterized Xis/RDF proteins belong to this family e.g. *E. coli* TorI (76), and the Xis proteins from *E. coli* phage Phi80 (77) and *Shigella flexneri* (78).

An alignment was made of $\Phi24_B$ Xis with other experimentally demonstrated or reliably predicted excisionase sequences, building on earlier lists (28,78). Extreme sequence diversity has often left doubts over the true homology of some excisionases (28), and the alignment was therefore limited to sequences with demonstrable homology, using sensitive profile–profile matching (40,41) to winged-helix excisionases such as lambda Xis and TorI. As well as phage_AlpA, these sequences belonged to, or resembled, several Pfam families: Excisionase like [PF07825; e.g. lambda phage Xis (27)], Tn916-Xis [PF09035 (45)], Putative excisionase [PF06806 (64)] and Regulatory phage protein Cox [PF10743 (79)]. Alignment (Supplementary Figure S1) of these sequences illustrated the extreme sequence diversity of excisionases with this architecture. Even within the common helix-turn-helix motif and the shared small 'wing' β-sheet sequence, conservation is very limited, and many members have N- or C-terminal extensions. This diversity is responsible for the difficulty previously encountered (28) and seen again in this work, of annotating excisionase proteins using conventional bioinformatic tools. Bootstrapped phylogenetic analysis of the alignment (Supplementary Figure S2) revealed few strongly supported nodes, unsurprising in view of the diversity of the sequences. In particular, $\Phi24_B$ Xis clustered reliably only with an unpublished, unannotated sequence from Stx2-converting Φ86 phage (Accession number: AB255436) from *E. coli* O86. This phage is a close relative of $\Phi24_B$ and its almost identical integrase shares the inverse orientation, in contrast, to most characterized lambdoid phages.

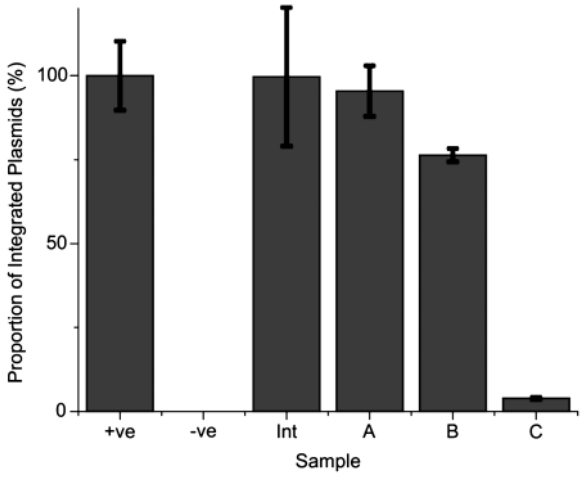

Figure 5. qPCR quantification of integration/excision. Proportion of total plasmids present that are in the integrated state (p$\Phi24_B$-*attLR*): (+ve) agarose gel purified p$\Phi24_B$-*attLR*; (−ve) p$\Phi24_B$-*attB* and p$\Phi24_B$-*attP* in the absence of either a phage or plasmid borne integrase; (Int) p$\Phi24_B$-*attB* and p$\Phi24_B$-*attP* in the presence of expressed $\Phi24_B$ integrase (Table 2, assay2 with arabinose); (**A–C**) p$\Phi24_B$-*attLR* in the presence of co-expressed arabinose-inducible $\Phi24_B$ integrase and excisionase at arabinose concentrations (w/v) of 0%, 0.002 and 0.2%, respectively (Table 2, assay5).

Experimental validation of excisionase function

Excisionase function was confirmed experimentally for the newly identified $\Phi24_B$ *xis* ORF by co-expression with $\Phi24_B$ *int* from a single expression plasmid construct, p$\Phi24_B$-IX, in the presence of the integrated p$\Phi24_B$-*attLR* plasmid *in situ* (Figure 4). The co-expressed proteins were able to effectively resolve p$\Phi24_B$-*attLR* into its constituent plasmids, resulting in cells harboring the expression construct plus the plasmids p$\Phi24_B$-*attB* and p$\Phi24_B$-*attP*, as observed by agarose gel electrophoresis (Figure 4B). Some residual p$\Phi24_B$-*attLR* remained in these cultures, though in lower quantities than the resolved plasmids. To obtain a quantitative measure of the efficiency of these reactions, an absolute qPCR method was devised to enumerate the levels of integrated p$\Phi24_B$-*attLR* plasmid compared to individual component plasmids (Figure 4A). Integration and excision reactions were consistently efficient and indisputably substantiate the claim that the proposed $\Phi24_B$ integrase and excisionase do indeed function as predicted (Figure 5).

A molecular model of $\Phi24_B$ Xis

The structure of *E. coli* TorI (44) was used as a template to model $\Phi24_B$ Xis. Although the HHpred-derived alignment matched only 15% of residues between the two proteins, modeling was facilitated by the existence of only a single one-residue deletion in $\Phi24_B$ Xis compared to TorI, which could be readily structurally accommodated. Ten models were constructed with MODELLER (54) and that with the best DOPE score (55) selected. The chosen model also had good stereochemical qualities including 87%

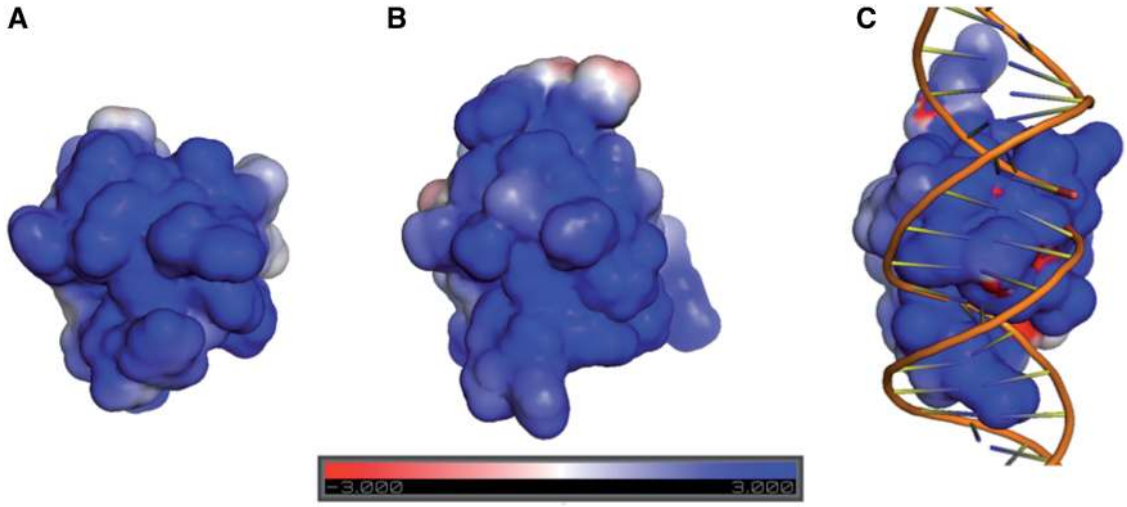

Figure 6. Electrostatic analysis of protein structures. The three structurally superimposed structures shown are (**A**) $\Phi24_B$ Xis model, (**B**) TorI (44) and (**C**) lambda Xis in complex with DNA (27). Solvent-accessible surfaces are colored blue (positive) to red (negative). Calculations were done with APBS (57).

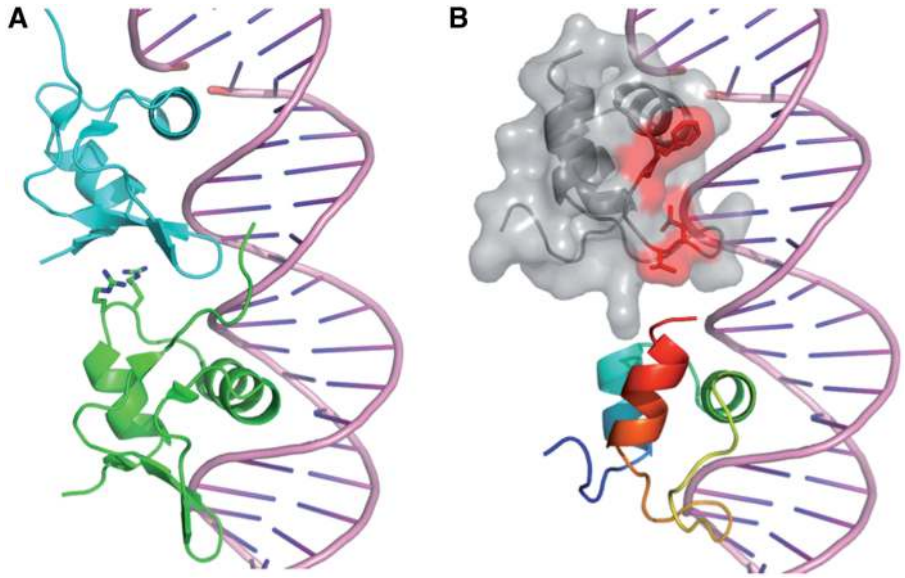

Figure 7. Comparison of lambda phage Xis micronucleoprotein filament-like DNA-bound structure and a hypothetical $\Phi24_B$ Xis model structure. (**A**) Adjacent subunits of the lambda phage Xis micronucleoprotein filament (27) with an interface loop highlighted with Arg13 and Arg14 side chains. (**B**) The selected model is superimposed on the same lambda phage Xis subunits. The lower subunit is coloured in a spectrum from blue N-terminus to red (incomplete) C-terminus. The upper subunit is shown as cartoon and semi-transparent molecular surface and is colored as gray except for the four exposed hydrophobic residues—Phe31, Pro32, Val35 and Leu36—highlighted by HotPatch (58) as a possible protein–protein interaction site which are colored red. The very C-terminal residues of $\Phi24_B$ Xis, not included in the model, could interact with that putative interaction site.

of residues in core areas of the Ramachandran plot (56). The C-terminal seven residues of $\Phi24_B$ Xis could not be modeled since they were not aligned with template by HHpred and are likely to adopt a different conformation: no regular secondary structure for this region is predicted in $\Phi24_B$ Xis, but the corresponding part of TorI is α-helical.

DNA-binding proteins often have a large positively charged, surface and we sought this feature on the $\Phi24_B$ Xis model. Indeed, one face of the Xis protein bears a pronounced positive charge (Figure 6A). This corresponds to the side of the protein structure that binds DNA in the lambda phage Xis crystal structure (Figure 6C) (27), which has been implicated by site-directed mutagenesis in DNA binding of TorI (44).

In view of the capacity of some Xis proteins—demonstrated or predicted (27)—to self-interact and form DNA-bound micronucleoprotein filaments, potential sites of protein–protein interaction on the $\Phi24_B$ Xis model were sought with HotPatch (58). For protein–protein interactions, exposed hydrophobic residues constitute the most reliable predictor of interaction sites. The

model of $\Phi24_B$ Xis produces a single, strong prediction comprising four solvent-exposed hydrophobic residues in close proximity—Phe31, Pro32, Val35 and Leu36 (Figure 7).

DISCUSSION

Previous examination of the $\Phi24_B$ genome sequence revealed the presence of a putative antirepressor gene possessing 37% amino acid identity to the well-characterized P22 antirepressor, Ant (Accession number: NP_059643) (20,25). It was also demonstrated qualitatively that the *ant* gene was expressed at very low levels in a quiescent lysogen culture (20). Alignment of the putative $\Phi24_B$ antirepressor protein with its P22 counterpart revealed significant sequence similarity primarily in the C-terminal domains (82% identity for the final 104 C-terminal residues). When expressed, P22 Ant is able to inactivate the phage repressor protein, analogous to the lambda CI repressor. This observation and the fact that we could measure expression of *ant* in the lysogen (20) led to speculation that $\Phi24_B$ Ant could alleviate CI repression sufficiently to allow superinfecting phages to integrate. However, the data presented here refute this hypothesis. No significant effect was observed on lysogen formation rates, either when superinfecting an isogenic *ant*-strain or when Ant was expressed from a plasmid in the host cells undergoing superinfection. On the other hand, when an *ant*-lysogen strain was induced into the lytic life cycle it was unable to effectively upregulate expression from the pR′ late genes promoter, in contrast to the wild-type with monitoring by bioluminescence assay (Figure 1C). Expression of Ant during induction almost completely complemented wild-type induction levels. Hence, it seems that although $\Phi24_B$ Ant may well, but not necessarily, act on CI thus leading to its deactivation/inhibition, the role of Ant in the phage life cycle is not associated with multiple lysogeny but rather the acceleration of derepression during lytic induction (Figure 1C).

The confirmed ability of the lambdoid phage $\Phi24_B$ to form multiple lysogens, following sequential infection of a single host (18,20), directly contradicts predictions based upon the well-characterized lambda immunity model, despite the presence in $\Phi24_B$ of an apparently intact lambda-like immunity region with equivalent repressor binding affinities (66,67,80). Here, we present data which reveal the mechanism by which $\Phi24_B$ is able to circumvent superinfection immunity and, more importantly, actively promote the incorporation of multiple prophages following primary infection (20). The $\Phi24_B$ model hinges on the discovery, from the annotated genome sequence (HM_208303), that the integrase gene is transcribed in an inverted orientation relative to λ (Figure 3A) (15) This fact, in conjunction with the discovery and characterization of a novel excisionase oriented in the same direction as λ *xis* (Figure 3A), allows us to predict the chain of events that occurs during superinfection. Integrase production is not repressed by the phage global repressor, CI (Figure 2) nor coupled to the lambdoid phage gene regulatory networks, but rather its expression is allowed to continue during stable lysogeny (Figure 2), presumably leading to an intracellular build up of Int. It is the accumulation of integrase in the cytoplasm, in conjunction with the lack of repression of incoming isogenic phage integrase production, which most likely accounts for the increased frequency of lysogen formation during superinfection compared to infection of a naïve host (20). Furthermore, as the excisionase is not produced from the $pInt_{24B}$ promoter, $\Phi24_B$ is able to maintain a state of stable lysogeny despite the constitutive expression of *int*, as *xis* expression is linked to a standard lambda prophage induction pathway. This is exemplified by the almost complete conversion of plasmids bearing *attP* and *attB* to the integrated form (Figures 4 and 5), when propagated in an uninduced $\Phi24_B$ lysogen. In summary, the evidence presented points to a clear mechanism for $\Phi24_B$ multiple lysogen production at a high rate, due to the fact that integrase is outside the control of global phage repression, however, prophage stability is maintained due to the orientation and lambdoid genetic regulatory strategy which leaves *xis* coupled to CI repressor control.

Identification of the $\Phi24_B$ excisionase was a non-trivial task as, despite careful investigation of the $\Phi24_B$ genome sequence, we were unable to identify any candidate ORFs likely to encode an excisionase gene in the expected area, and Blastn searches of the sequences surrounding the *int* gene against the non-redundant databases failed to elucidate any possible Xis coding sequences. This led us to consider the possibility that there may be no such gene present in the phage genome. Although there have been no reported cases of infective bacteriophages able to catalyze integration and excision with an integrase alone, such a situation has been described for a uropathogenic *E. coli* pathogenicity island (30,31). However, in light of the fact that resolution of p$\Phi24_B$-*attLR* to its constituent plasmids was not possible when integrase alone was expressed from an inducible plasmid while excision events were detected when the $\Phi24_B$ prophage was present, a systematic location-targeted strategy was successfully employed. Distant homology of the candidate Xis protein sequence with the Phage_AlpA family, already containing several known excisionases, bore out our initial suspicions based on its genomic context. A molecular model confirmed that $\Phi24_B$ Xis protein adopts a winged-helix fold.

Interestingly, excisionase proteins with the winged-helix fold appear to function in diverse ways. In the archetypal Lambda phage Xis, from Pfam family 'Excisionase-like', binds directly to DNA, forming a micronucleoprotein filament which bends the DNA duplex in a way predicted to facilitate the excision process (27). Data suggest that the Tn916 Xis may function similarly (27). *Escherichia coli* TorI, from Pfam family phage_AlpA acts as a response regulator inhibitor, binding not only to DNA (44) but also to the DNA-binding domain of the TorR protein (76). Although this protein–protein interaction does not affect the DNA-binding capacity of TorR, it is thought to impede recruitment of RNA polymerase to the *torC* promoter. Finally, the AlpA protein acts as a transcription factor for the *int* gene of the phage CP4-57 in *E. coli* K-12

(81,82), thereby affecting excision by a third variant mechanism.

DNA binding is a common feature of all these excisionases, and so it is no surprise that the model of $\Phi24_B$ Xis bears a characteristic positively charged surface (Figure 6). Structure-based predictors of DNA-binding capacity—DB-MOM (59) and PRO-DNA (60)—confirm that $\Phi24_B$ Xis should bind DNA. Attempts to predict further details of the molecular mechanism of $\Phi24_B$ Xis by phylogenomic analysis failed since boots-trapped trees did not reliably group this Xis with other experimentally studied excisionases (Supplementary Figure S2). However, the $\Phi24_B$ Xis model allowed us to address one aspect of function, namely the ability to form micronucleoprotein filaments. Inspection of the structure of phage lambda micronucleoprotein filament structure (Figure 7A) highlights the role of the loop containing Arg13 and Arg14 in forming inter-subunit contacts. The corresponding loops in $\Phi24_B$ Xis (Figure 7B) and Tn916 Xis (not shown) are shorter and, without significant re-arrangement, appear to be too short to form similar inter-actions. However, seven residues at the C-terminus of $\Phi24_B$ Xis could not be modeled since they did not align reliably with the template. Intriguingly, the C-terminus of the incomplete model clearly shows that the missing residues could interact with the neighboring subunit at exactly the region picked out as a potential protein–protein interaction site. DNA purified from cells expressing $\Phi24_B$ Xis could not be cut with restriction endonucleases without a significant degradation of DNA: no bands were seen on subsequent agarose gels, only smearing (Figure 4B). This observation offers cir-cumstantial support for the notion that $\Phi24_B$ Xis binds DNA as micronucleoprotein filaments thereby destabilizing the duplex structure and increasing its susceptibility to degradation.

SUPPLEMENTARY DATA

Supplementary Data are available at NAR Online.

FUNDING

Funding for open access charge: Funding for the work preceding this article was obtained from the Biotechnology and Biological Science Research Council of the U.K. The work detailed in this article was funded by its authors.

Conflict of interest statement. None declared.

REFERENCES

1. Riley,L.W., Remis,R.S., Helgerson,S.D., McGee,H.B., Wells,J.G., Davis,B.R., Hebert,R.J., Olcott,E.S., Johnson,L.M., Hargrett,N.T. *et al*. (1983) Hemorrhagic colitis associated with a rare *Escherichia coli* serotype. *N. Engl. J. Med*., **308**, 681–685.
2. Ziebell,K., Steele,M., Zhang,Y., Benson,A., Taboada,E.N., Laing,C., McEwen,S., Ciebin,B., Johnson,R. and Gannon,V. (2008) Genotypic characterization and prevalence of virulence factors among Canadian *Escherichia coli* O157:H7 strains. *Appl. Environ. Microbiol*., **74**, 4314–4323.
3. Akashi,S., Joh,K., Tsuji,A., Ito,H., Hoshi,H., Hayakawa,T., Ihara,J., Abe,T., Hatori,M., Mori,T. *et al*. (1994) A severe outbreak of haemorrhagic colitis and haemolytic uraemic syndrome associated with *Escherichia coli* O157:H7 in Japan. *Eur. J. Pediatr*., **153**, 650–655.
4. Cowden,J.M., Ahmed,S., Donaghy,M. and Riley,A. (2001) Epidemiological investigation of the central Scotland outbreak of *Escherichia coli* O157 infection, November to December 1996. *Epidemiol. Infect*., **126**, 335–341.
5. Caprioli,A., Tozzi,A.E., Rizzoni,G. and Karch,H. (1997) Non-O157 Shiga toxin-producing *Escherichia coli* infections in Europe. *Emerg. Infect. Dis*., **3**, 578–579.
6. Prado,V., Martinez,J., Arellano,C. and Levine,M.M. (1997) Temporal variation of genotypes and serotypes of enterohemorrhagic *E coli* isolated from Chilean children with intestinal infections or hemolytic uremic syndrome. *Rev. Med. Chil*., **125**, 291–297.
7. Werber,D., Fruth,A., Liesegang,A., Littmann,M., Buchholz,U., Prager,R., Karch,H., Breuer,T., Tschape,H. and Ammon,A. (2002) A multistate outbreak of Shiga toxin-producing *Escherichia coli* O26:H11 infections in Germany, detected by molecular subtyping surveillance. *J. Infect. Dis*., **186**, 419–422.
8. Calderon,V.E., Chang,Q., McDermott,M., Lytle,M.B., McKee,G., Rodriguez,K., Rasko,D.A., Sperandio,V. and Torres,A.G. (2009) Outbreak caused by cad-Negative Shiga toxin-producing *Escherichia coli* O111, Oklahoma. *Foodborne Pathog. Dis*., **7**, 107–109.
9. Sonntag,A.K., Prager,R., Bielaszewska,M., Zhang,W., Fruth,A., Tschape,H. and Karch,H. (2004) Phenotypic and genotypic analyses of enterohemorrhagic *Escherichia coli* O145 strains from patients in Germany. *J. Clin. Microbiol*., **42**, 954–962.
10. O'Brien,A.D., Newland,J.W., Miller,S.F., Holmes,R.K., Smith,H.W. and Formal,S.B. (1984) Shiga-like toxin-converting phages from *Escherichia coli* strains that cause hemorrhagic colitis or infantile diarrhea. *Science*, **226**, 694–696.
11. O'Brien,A.D., LaVeck,G.D., Thompson,M.R. and Formal,S.B. (1982) Production of *Shigella dysenteriae* type 1-like cytotoxin by Escherichia coli. *J. Infect. Dis*., **146**, 763–769.
12. Allison,H.E. (2007) Stx-phages: drivers and mediators of the evolution of STEC and STEC-like pathogens. *Fut. Microbiol*., **2**, 165–174.
13. Gamage,S.D., Patton,A.K., Strasser,J.E., Chalk,C.L. and Weiss,A.A. (2006) Commensal bacteria influence *Escherichia coli* O157:H7 persistence and Shiga toxin production in the mouse intestine. *Infect. Immun*., **74**, 1977–1983.
14. Court,D.L., Oppenheim,A.B. and Adhya,S.L. (2007) A new look at bacteriophage {lambda} genetic networks. *J. Bacterio*., **189**, 298–304.
15. Ptashne,M. (2004) A genetic switch: phage lambda revisited, 3rd edn. Cold Spring Harbor Laboratory Press, Cold Spring Harbor.
16. Rice,P.A. (2005) Resolving integral questions in site-specific recombination. *Nat. Struct. Mol. Biol*., **12**, 641.
17. Chen,Y., Narendra,U., Iype,L.E., Cox,M.M. and Rice,P.A. (2000) Crystal structure of a Flp recombinase-Holliday junction complex: assembly of an active oligomer by helix swapping. *Mol. Cell*, **6**, 885.
18. Allison,H.E., Sergeant,M.J., James,C.E., Saunders,J.R., Smith,D.L., Sharp,R.J., Marks,T.S. and McCarthy,A.J. (2003) Immunity profiles of wild-type and recombinant Shiga-like toxin-encoding bacteriophages and characterization of novel double lysogens. *Infect. Immun*., **71**, 3409–3418.
19. Serra-Moreno,R., Jofre,J. and Muniesa,M. (2008) The CI repressors of Shiga toxin-converting prophages are involved in coinfection of *Escherichia coli* strains, which causes a down regulation in the production of Shiga toxin 2. *J. Bacteriol*., **190**, 4722–4735.
20. Fogg,P.C., Gossage,S.M., Smith,D.L., Saunders,J.R., McCarthy,A.J. and Allison,H.E. (2007) Identification of multiple integration sites for Stx-phage Phi24B in the *Escherichia coli* genome, description of a novel integrase and evidence for a functional anti-repressor. *Microbiol*., **153**, 4098–4110.
21. Botstein,D. (1980) A theory of modular evolution for bacteriophages. *Ann. N. Y. Acad. Sci*., **354**, 484–490.

22. Brussow,H., Canchaya,C. and Hardt,W.-D. (2004) Phages and the evolution of bacterial pathogens: from genomic rearrangements to lysogenic conversion. *Microbiol. Mol. Biol. Rev.*, **68**, 560–602.
23. Botstein,K., Lew,K.K., Jarvik,V. and Swanson,C.A. (1975) Role of antirepressor in the bipartite control of repression and immunity by bacteriophage P22. *J. Mol. Biol.*, **91**, 439–462.
24. Susskind,M.M. and Botstein,D. (1975) Mechanism of action of Salmonella phage P22 antirepressor. *J. Mol. Biol.*, **98**, 413–424.
25. Susskind,M.M. and Botstein,D. (1978) Molecular genetics of bacteriophage P22. *Microbiol. Rev.*, **42**, 385–413.
26. Little,J.W. (1984) Autodigestion of lexA and phage lambda repressors. *PNAS USA*, **81**, 1375–1379.
27. Abbani,M.A., Papagiannis,C.V., Sam,M.D., Cascio,D., Johnson,R.C. and Clubb,R.T. (2007) Structure of the cooperative Xis-DNA complex reveals a micronucleoprotein filament that regulates phage lambda intasome assembly. *PNAS USA*, **104**, 2109–2114.
28. Lewis,J.A. and Hatfull,G.F. (2001) Control of directionality in integrase-mediated recombination: examination of recombination directionality factors (RDFs) including Xis and Cox proteins. *Nucleic Acids Res.*, **29**, 2205–2216.
29. Franz,B. and Landy,A. (1995) The Holliday junction intermediates of lambda integrative and excisive recombination respond differently to the bending proteins integration host factor and excisionase. *EMBO J.*, **14**, 397–406.
30. Hochhut,B., Wilde,C., Balling,G., Middendorf,B., Dobrindt,U., Brzuszkiewicz,E., Gottschalk,G., Carniel,E. and Hacker,J. (2006) Role of pathogenicity island-associated integrases in the genome plasticity of uropathogenic *Escherichia coli* strain 536. *Mol. Microbiol.*, **61**, 584–595.
31. Wilde,C., Mazel,D., Hochhut,B., Middendorf,B., Roux,F.L., Carniel,E., Dobrindt,U. and Hacker,J. (2008) Delineation of the recombination sites necessary for integration of pathogenicity islands II and III into the *Escherichia coli* 536 chromosome. *Mol. Microbiol.*, **68**, 139–151.
32. Qazi,S.N.A., Counil,E., Morrissey,J., Rees,C.E.D., Cockayne,A., Winzer,K., Chan,W.C., Williams,P. and Hill,P.J. (2001) *agr* expression precedes escape of internalized *Staphylococcus aureus* from the host endosome. *Infect. Immun.*, **69**, 7074–7082.
33. Matsushiro,A., Sato,K., Miyamoto,H., Yamamura,T. and Honda,T. (1999) Induction of prophages of enterohemorrhagic *Escherichia coli* O157:H7 with norfloxacin. *J. Bacteriol.*, **181**, 2257–2260.
34. Rooks,D.J., Yan,Y., McDonald,J.E., Woodward,M.J., McCarthy,A.J. and Allison,H.E. (2010) Development and validation of a qPCR-based method for quantifying Shiga toxin-encoding and other lambdoid bacteriophages. *Environ. Microbiol.*, **12**, 1194–1204.
35. Livak,K.J. and Schmittgen,T.D. (2001) Analysis of relative gene expression data using real-time quantitative PCR and the 2-[Delta][Delta]CT method. *Methods*, **25**, 402–408.
36. Blattner,F.R., Plunkett,G. III, Bloch,C.A., Perna,N.T., Burland,V., Riley,M., Collado-Vides,J., Glasner,J.D., Rode,C.K., Mayhew,G.F. *et al.* (1997) The complete genome sequence of *Escherichia coli* K-12. *Science*, **277**, 1453–1462.
37. Altschul,S.F., Madden,T.L., Schaffer,A.A., Zhang,J.H., Zhang,Z., Miller,W. and Lipman,D.J. (1997) Gapped BLAST and PSI-BLAST: a new generation of protein database search programs. *Nucleic Acids Res.*, **25**, 3389–3402.
38. Wheeler,D.L., Barrett,T., Benson,D.A., Bryant,S.H., Canese,K., Chetvernin,V., Church,D.M., DiCuccio,M., Edgar,R., Federhen,S. *et al.* (2007) Database resources of the National Center for Biotechnology Information. *Nucleic Acids Res.*, **35**, D5–D12.
39. Hunter,S., Apweiler,R., Attwood,T.K., Bairoch,A., Bateman,A., Binns,D., Bork,P., Das,U., Daugherty,L., Duquenne,L. *et al.* (2009) InterPro: the integrative protein signature database. *Nucleic Acids Res.*, **37**, D211–D215.
40. Soding,J. (2005) Protein homology detection by HMM-HMM comparison. *Bioinformatics*, **21**, 951–960.
41. Soding,J., Biegert,A. and Lupas,A.N. (2005) The HHpred interactive server for protein homology detection and structure prediction. *Nucleic Acids Res.*, **33**, W244–248.
42. Finn,R.D., Mistry,J., Tate,J., Coggill,P., Heger,A., Pollington,J.E., Gavin,O.L., Gunasekaran,P., Ceric,G., Forslund,K. *et al.* (2010) The Pfam protein families database. *Nucleic Acids Res.*, **38**, D211–D222.
43. Berman,H., Henrick,K., Nakamura,H. and Markley,J.L. (2007) The worldwide Protein Data Bank (wwPDB): ensuring a single, uniform archive of PDB data. *Nucleic Acids Res.*, **35**, D301–D303.
44. Elantak,L., Ansaldi,M., Guerlesquin,F., Mejean,V. and Morelli,X. (2005) Structural and genetic analyses reveal a key role in prophage excision for the TorI response regulator inhibitor. *J. Biol. Chem.*, **280**, 36802–36808.
45. Abbani,M., Iwahara,M. and Clubb,R.T. (2005) The structure of the excisionase (Xis) protein from conjugative transposon Tn916 provides insights into the regulation of heterobivalent tyrosine recombinases. *J. Mol. Biol.*, **347**, 11–25.
46. Konagurthu,A.S., Whisstock,J.C., Stuckey,P.J. and Lesk,A.M. (2006) MUSTANG: a multiple structural alignment algorithm. *Proteins*, **64**, 559–574.
47. Waterhouse,A.M., Procter,J.B., Martin,D.M., Clamp,M. and Barton,G.J. (2009) Jalview Version 2–a multiple sequence alignment editor and analysis workbench. *Bioinformatics*, **25**, 1189–1191.
48. Edgar,R.C. (2004) MUSCLE: multiple sequence alignment with high accuracy and high throughput. *Nucleic Acids Res.*, **32**, 1792–1797.
49. Tamura,K., Dudley,J., Nei,M. and Kumar,S. (2007) MEGA4: Molecular Evolutionary Genetics Analysis (MEGA) software version 4.0. *Mol. Biol. Evol.*, **24**, 1596–1599.
50. Felsenstein,J. (1985) Confidence-limits on phylogenies - an approach using the bootstrap. *Evolution*, **39**, 783–791.
51. Zuckerkandl,E. and Pauling,L. (1965) In Bryson,V. and Vogel,H.J. (eds), *Evolving Genes and Proteins*. Academic Press, New York, pp. 97–166.
52. Nei,M. and Kumar,S. (2000) *Molecular Evolution and Phylogenetics*. Oxford University Press, New York.
53. Saitou,N. and Nei,M. (1987) The neighbor-joining method: a new method for reconstructing phylogenetic trees. *Mol. Biol. Evol.*, **4**, 406–425.
54. Sali,A. and Blundell,T.L. (1993) Comparative protein modelling by satisfaction of spatial restraints. *J. Mol. Biol.*, **234**, 779–815.
55. Shen,M.Y. and Sali,A. (2006) Statistical potential for assessment and prediction of protein structures. *Protein Sci.*, **15**, 2507–2524.
56. Laskowski,R.A., Macarthur,M.W., Moss,D.S. and Thornton,J.M. (1993) Procheck – a program to check the stereochemical quality of protein structures. *J. Appl. Crystall.*, **26**, 283–291.
57. Baker,N.A., Sept,D., Joseph,S., Holst,M.J. and McCammon,J.A. (2001) Electrostatics of nanosystems: application to microtubules and the ribosome. *PNAS USA*, **98**, 10037–10041.
58. Pettit,F.K., Bare,E., Tsai,A. and Bowie,J.U. (2007) HotPatch: a statistical approach to finding biologically relevant features on protein surfaces. *J. Mol. Biol.*, **369**, 863–879.
59. Ahmad,S. and Sarai,A. (2004) Moment-based prediction of DNA-binding proteins. *J Mol Biol*, **341**, 65–71.
60. Bhardwaj,N., Langlois,R.E., Zhao,G. and Lu,H. (2005) Kernel-based machine learning protocol for predicting DNA-binding proteins. *Nucleic Acids Res.*, **33**, 6486–6493.
61. Krissinel,E. and Henrick,K. (2004) Secondary-structure matching (SSM), a new tool for fast protein structure alignment in three dimensions. *Acta Crystallogr. D. Biol. Crystallogr.*, **60**, 2256–2268.
62. DeLano,W.L. (2002) PyMOL. www.pymol.org [8 October 2010, date last accessed].
63. Strauch,E., Hammerl,J.A., Konietzny,A., Schneiker-Bekel,S., Arnold,W., Goesmann,A., Puhler,A. and Beutin,L. (2008) Bacteriophage 2851 is a prototype phage for dissemination of the Shiga toxin variant gene 2c in *Escherichia coli* O157:H7. *Infect. Immun.*, **76**, 5466–5477.
64. Plunkett,G. III, Rose,D.J., Durfee,T.J. and Blattner,F.R. (1999) Sequence of Shiga toxin 2 phage 933W from *Escherichia coli* O157:H7: Shiga toxin as a phage late-gene product. *J. Bacteriol.*, **181**, 1767–1778.
65. Evans,T., Bowers,R.G. and Mortimer,M. (2007) Modelling the stability of Stx lysogens. *J. Theor. Biol.*, **248**, 241–250.
66. Koudelka,A.P., Hufnagel,L.A. and Koudelka,G.B. (2004) Purification and characterization of the repressor of the Shiga

toxin-encoding bacteriophage 933W: DNA binding, gene regulation, and autocleavage. *J. Bacteriol.*, **186**, 7659–7669.
67. Tyler,J.S., Mills,M.J. and Friedman,D.I. (2004) The operator and early promoter region of the Shiga toxin type 2-encoding bacteriophage 933W and control of toxin expression. *J. Bacteriol.*, **186**, 7670–7679.
68. Reese,M.G. (2001) Application of a time-delay neural network to promoter annotation in the *Drosophila melanogaster* genome. *Comp. Chem.*, **26**, 51–56.
69. Rao,L., Ross,W., Appleman,J.A., Gaal,T., Leirmo,S., Schlax,P.J., Record,M.T. Jr and Gourse,R.L. (1994) Factor independent activation of *rrnB* P1. An "extended" promoter with an upstream element that dramatically increases promoter strength. *J. Mol. Biol.*, **235**, 1421–1435.
70. Husnain,S.I. and Thomas,M.S. (2008) The UP element is necessary but not sufficient for growth rate-dependent control of the *Escherichia coli guaB* promoter. *J. Bacteriol.*, **190**, 2450–2457.
71. Estrem,S.T., Gaal,T., Ross,W. and Gourse,R.L. (1998) Identification of an UP element consensus sequence for bacterial promoters. *PNAS USA*, **95**, 9761–9766.
72. Typas,A. and Hengge,R. (2005) Differential ability of sigma(s) and sigma70 of *Escherichia coli* to utilize promoters containing half or full UP-element sites. *Mol. Microbiol.*, **55**, 250–260.
73. Schiex,T., Gouzy,J., Moisan,A. and de Oliveira,Y. (2003) FrameD: a flexible program for quality check and gene prediction in prokaryotic genomes and noisy matured eukaryotic sequences. *Nucleic Acids Res.*, **31**, 3738–3741.
74. Groth,A.C. and Calos,M.P. (2004) Phage integrases: biology and applications. *J. Mol. Biol.*, **335**, 667–678.
75. Rajeev,L., Malanowska,K. and Gardner,J.F. (2009) Challenging a paradigm: the role of DNA homology in tyrosine recombinase reactions. *Microbiol. Mol. Biol. Rev.*, **73**, 300–309.
76. Ansaldi,M., Theraulaz,L. and Mejean,V. (2004) Torl, a response regulator inhibitor of phage origin in *Escherichia coli*. *PNAS USA*, **101**, 9423–9428.
77. Leong,J.M., Nunesduby,S.E., Oser,A.B., Lesser,C.F., Youderian,P., Susskind,M.M. and Landy,A. (1986) Structural and regulatory divergence among site-specific recombination genes of lambdoid phage. *J. Mol. Biol.*, **189**, 603–616.
78. Luck,S.N., Turner,S.A., Rajakumar,K., Adler,B. and Sakellaris,H. (2004) Excision of the Shigella resistance locus pathogenicity island in *Shigella flexneri* is stimulated by a member of a new subgroup of recombination directionality factors. *J. Bacteriol.*, **186**, 5551–5554.
79. Esposito,D. and Scocca,J.J. (1994) Identification of an HP1 phage protein required for site-specific excision. *Mol. Microbiol.*, **13**, 685–695.
80. Fattah,K.R., Mizutani,S., Fattah,F.J., Matsushiro,A. and Sugino,Y. (2000) A comparative study of the immunity region of lambdoid phages including Shiga-toxin-converting phages: molecular basis for cross immunity. *Genes Genet. Syst.*, **75**, 223–232.
81. Kirby,J.E., Trempy,J.E. and Gottesman,S. (1994) Excision of a P4-like cryptic prophage leads to Alp protease expression in *Escherichia coli*. *J. Bacteriol.*, **176**, 2068–2081.
82. Trempy,J.E., Kirby,J.E. and Gottesman,S. (1994) Alp suppression of Lon: dependence on the *slpA* gene. *J. Bacteriol.*, **176**, 2061–2067.
83. James,C.E., Stanley,K.N., Allison,H.E., Flint,H.J., Stewart,C.S., Sharp,R.J., Saunders,J.R. and McCarthy,A.J. (2001) Lytic and lysogenic infection of diverse *Escherichia coli* and Shigella strains with a verocytotoxigenic bacteriophage. *Appl. Environ. Microbiol.*, **67**, 4335–4337.
84. Mount,D.W. (1977) A mutant of *Escherichia coli* showing constitutive expression of the lysogenic induction and error-prone DNA repair pathways. *PNAS USA*, **74**, 300–304.
85. Penfold,R.J. and Pemberton,J.M. (1992) An improved suicide vector for construction of chromosomal insertion mutations in bacteria. *Gene*, **118**, 145–146.
86. Kaniga,K., Delor,I. and Cornelis,G.R. (1991) A wide-host-range suicide vector for improving reverse genetics in Gram-negative bacteria: inactivation of the *blaA* gene of *Yersinia enterocolitica*. *Gene*, **109**, 137–141.
87. Kumar,S., Nei,M., Dudley,J. and Tamura,K. (2008) MEGA: a biologist-centric software for evolutionary analysis of DNA and protein sequences. *Brief Bioinform.*, **9**, 299–306.
88. Fogg,P.C., Allison,H.E., Saunders,J.R. and McCarthy,A.J. (2010) Bacteriophage lambda: a paradigm revisited. *J. Virol.*, **84**, 6876–6879.